PROCEEDINGS of
CHEF 2013

EndoTOFPET-US - A Miniaturised Calorimeter for Endoscopic Time-of-Flight Positron Emission Tomography

Milan Zvolský* **on behalf of the EndoTOFPET-US Collaboration**
DESY Hamburg, Germany
E-mail: milan.zvolsky@desy.de

In the scope of the EndoTOFPET-US project, a novel multimodal device for Ultrasound (US) Endoscopy and Positron Emission Tomography (PET) is being developed. The project aims at detecting and quantifying morphologic and functional markers and developing new biomarkers for pancreas and prostate oncology. Exploiting the Time-of-Flight (TOF) information of the gamma rays allows for a more sensitive, more precise and lower radiation-dose imaging and intervention on small internal structures. The detection of the gamma rays is realised with the help of scintillator crystals with Silicon Photomultiplier (SiPM) read-out, aiming at a coincidence time resolution of 200 ps and a spatial resolution of 1 mm. For the endoscopic detector, digital SiPMs are utilised for the first time in an instrument planned for clinical applications. The functionality of the instrument as well as the challenges that accompany the high level of miniaturisation of the endoscopic detector and the asymmetric and variable geometry of the system, are presented. The demands on the system involve the fields of scintillating crystals, ultra-fast photon detection, highly integrated electronics, system integration as well as image reconstruction. The design of the system, the status of the the single detector components and the integration plans are discussed.

Calorimetry for High Energy Frontiers - CHEF 2013,
April 22-25, 2013
Paris, France

*Speaker.

1. Introduction

Inspired by our expertise in high-energy physics calorimetry[1], such as the CMS calorimeter, which involves scintillation crystals, silicon photomultipliers and front-end electronics, we aim at commissioning a miniaturised calorimeter for endoscopic positron emission tomography (PET). The prospect of the EndoTOFPET-US project [2] [1] is the development of a novel multimodal imaging device for ultrasound (US) and time-of-flight PET for detecting and quantifying morphologic and functional markers as well as establishing and testing new biomarkers for pancreas and prostate carcinoma [2, 3]. At the same time this tool is supposed to provide an intra-operative guide for prostate and pancreas surgery. This is achieved by mounting a PET detector head on a commercially available US endoscope in combination with an outer detector plate located next to the body. Radio-labelled biomarkers are injected into the patient and undergo β^+ decay, leading to two back-to-back photons with an energy of 511 keV each. These photons are detected in coincidence by the endoscopic and the external detector.

The main reason for exploiting the endoscopic imaging approach is that the organ under study is surrounded by organs with a high metabolic uptake, such as liver, duodenum and gall bladder in case of the pancreas, and the bladder in case of the prostate. If one part of the PET detector is located in the direct proximity of the organ under study and provides time-of-flight (TOF) information, one is able to narrow down the region of interest and thus significantly reduce the background from neighbouring organs. Pancreas cancer is practically symptom-free during its early stages so that it often already spread to other organs when discovered, leading to highly adverse 5-year survival rates of around 8 % [4]. Prostate cancer, on the other hand, is among the most frequently diagnosed cancer for males, whereas survival rates are very good if diagnosed and treated sufficiently early. Being able to produce highly-resolved and low-noise functional (metabolic) images, fused with the anatomical information from the ultrasound transducer, allows for an earlier detection and thus a higher healing probability of prostatic and pancreatic carcinoma.

The challenges that come along with building and commissioning such a detector device involve the extreme miniaturisation of the endoscopic PET head and highly integrated electronics as well as the ultra-fast detection of photons in order to allow TOF measurements. Another challenge is the image reconstruction for a limited-angle, free-hand PET detector that incorporates TOF information and provides on-line images with a design spatial resolution of 1 mm FWHM.

The aim of this project is to achieve a coincidence time resolution (CTR) of 200 ps FWHM which corresponds to a flight distance of approximately 3 cm. This is realised by utilising fast inorganic scintillator crystals, read out by ultra-fast silicon photomultipliers (SiPMs). SiPMs are photon counting devices consisting of avalanche photodiodes operated in Geiger mode. Due to their high gain they are sensitive to single-photon hits which is crucial for the envisaged CTR.

[1] The project partners are involved in collaborations such as the CMS calorimeter at the Large Hadron Collider (LHC) as well as the CALICE calorimeter for the International Linear Collider (ILC).

[2] The EndoTOFPET-US consortium consists of six universities, three hospitals as well as three companies. See `https://endotofpet-us.web.cern.ch/endotofpet-us/partners.html` for a list of the project partners.

2. Detector Design

2.1 Endoscopic Detector

In case of the prototype for the prostate case, the endoscopic PET detector is mounted on a commercially available ultrasound (US) endoscope (Hitachi EUP-U533). Due to the immediate vicinity of the detector to the organ under study, a high granularity is crucial in order to guarantee excellent spatial resolution. On the other hand, due to anatomical constraints, the PET head extension must not exceed a volume of $23 \times 23 \times 40$ mm^3. On this volume, 324 detector channels are placed: The detector consists of two matrices of 9×18 LYSO scintillator crystals from Proteus with a size of $0.71 \times 0.71 \times 15$ mm^3 coupled to multi-channel digital SiPMs (md-SiPMs). Besides, the PET head extension houses the printed circuit board (PCB) as well as a cooling system and possibly an electromagnetic tracking sensor, as can be seen in Fig. 1 (left). The endoscope for the pancreas case will be equipped with only one 9×18 crystal matrix.

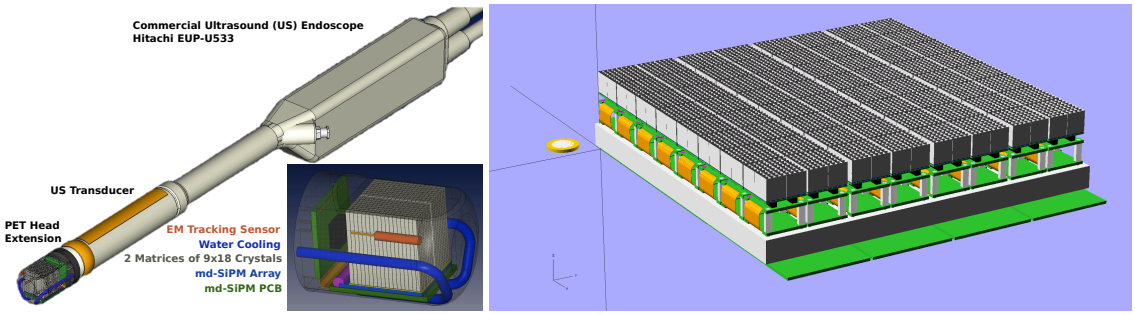

Figure 1: (*left*) Sketch of the design of the endoscopic ultrasound endoscope with the PET head extension. The inlet shows a zoom of the PET head, depicting the crystal matrices, md-SiPMs, PCB and cooling pipes. (*right*) CAD drawing of the current design of the external PET detector plate.The green plate underneath the detector depicts the front-end boards. Above that, an aluminium plate (grey) houses the cooling and mechanically fixes the printed circuit boards (PCBs) on which the ASICS are mounted. The uppermost structure symbolises the crystal matrices and the SiPM arrays.

2.2 External Detector Plate

The photons impinging on the endoscopic probe are detected in coincidence with an external detector plate which is located in the direct proximity of the patient. It is divided into 256 modules, each of which is assembled from a matrix of 4×4 LYSO crystals from Crystal Photonics Inc. (CPI) that are separated by 100 μm thick 3M Vikuiti reflector foil. The crystals have a size of $3.5 \times 3.5 \times 15$ mm^3, leading to a total number of 4096 single crystals on an area of 23×23 cm^2. Each crystal matrix is read out by an array of 4×4 discrete analog SiPMs. Dedicated fast 64-channel application specific integrated circuits (ASICs) are mounted directly on the detector plate in order to optimise the timing properties. Besides, an aluminium plate with an integrated water pipe will be embedded in the detector housing in order to cool the front-end boards (FEBs) and ASICs, c.f. Fig. 1 (right). The detector will be held by a robotic arm that allows for the movement in concordance with the endoscope movement as well as the precise tracking of its position.

2.3 Data Acquisition (DAQ)

The external plate houses eight front-end boards (FEBs), each of which accommodates eight 64-channel ASICs as well as a field programmable gate array (FPGA). The signals from the detector channels are transferred to the ASICs via flexible printed circuits. The FEB FPGA concentrates the digital output of the ASICs and transmits them to the DAQ card via a HDMI cable, c.f. Fig. 2 (left). The maximum event rate is 160 kHz per channel and 10 MHz per ASIC [5] which covers the expected event rate of 40 MHz. The events from the probe's md-SiPMs are read out by a small FPGA which is mounted directly on the probe. The maximum event rate for the probe is 625 kHz. The DAQ system uses a PCIe card, installed at the same bedside workstation that also hosts the computers for the image reconstruction, tracking and slow control. The card merges the data from the external plate and the probe and performs a coarse event selection of coincidence candidates, using a 12.5 ns wide coincidence window. This selection reduces the event rate to 350 kHz while ensuring that no interesting events are discarded. The DAQ software then extracts the precise energy and time information from the events, reconstructs in-detector Compton scattering and performs the final coincidence sorting. With a rate of less than 50 kHz the data is then processed to the image reconstruction software in list-mode format, along with the information from the ultrasound as well as the tracking data of probe and plate. The steps of the event processing and DAQ chain are sketched in Fig. 2 (right).

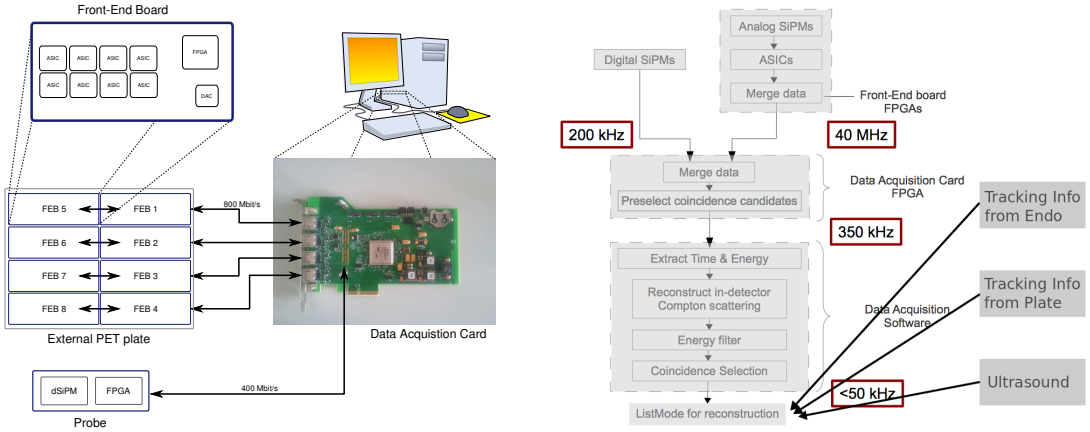

Figure 2: (*left*) Data acquisition (DAQ) system components [5]. (*right*) Flowchart of the DAQ and event processing chain.

2.4 Software and Hardware Integration

It is foreseen that two separate computers are housed by a bedside cart, one of which is responsible for the DAQ as well as the image reconstruction. A second PC is responsible for the tracking, communication and visualisation of the images, which involves the co-registration of PET and US images and the user interface. In order to control the communication between the multiple imaging and tracking devices, CAMPCom, a lightweight and portable communication framework for multimodal image-guided therapy [6, 7] has been developed for the EndoTOFPET-US project. The communication framework involves the full monitoring and quality control of all processes and enables the slow control.

Due to its application in an operating room, special demands on sterility, security and mobility need to be warranted for all hardware components. After cleaning, the ultrasound transducer is covered by a sterile latex probe cover. Moreover, strict temperature and leakage current limits must be met by the devices, especially the endoscope which is in direct contact with the patient [8].

For the tracking of the endoscope two different approaches come into consideration. Electromagnetic tracking can reach an accuracy of 3.83 ± 6.43 mm based on electromagnetic servoing [9]. Hybrid optic and electromagnetic tracking approaches are currently investigated and hold promising preliminary results with an approximate accuracy of 1.5-2 mm.

3. Single Component Characterisation

3.1 Scintillation crystals

A photo of crystal samples for internal probe and external plate are shown in Fig. 3 (left). The LY of the crystal matrices is measured by coupling the matrices to a photomultiplier tube (PMT) since measuring the energy resolution with a SiPM is not optimal due to its non-linear response. For the external plate the average LY amounts to 33000 Ph/MeV ($\pm 5\%$) when wrapping the crystal matrices with Vikuiti reflector foil and using optical grease to couple them to the PMT. This is more that four times higher than in the dry-contact and non-wrapped configuration. The spread in LY among the different crystals of a matrix is $\approx 10\%$. The average energy resolution of the whole matrix measures approximately $(20 \pm 7)\%$, sufficient to separate photo events from Compton-scattered events, c.f. Fig. 3 (right). The optical cross talk within a crystal matrix is less that 5 % which is lower than the electronic cross talk and noise and which can easily be suppressed by setting a low energy threshold.

The average LY of the 9×18 matrix for the internal probe coupled with dry contact to a PMT and Vikuiti-covered back is approximately 12000 Ph/MeV [10] which can be increased by a factor of 2.3 by using optical grease between PMT and crystal. The average energy resolution for this matrix amounts $\approx 18\%$. An automated LY measurement setup has been built to characterise the 256 crystal matrices fast and reproducibly [11].

The timing properties of the crystal matrices coupled to analog SiPMs are measured with the time-over-threshold method using an ultra-fast amplifier-discriminator chip NINO. The coincidence time resolution (CTR) between one matrix of the outer plate and one single crystal of the internal probe can deliver a CTR down to 220 ps [12].

3.2 Analog SiPMs

The SiPMs chosen for the external plate are arrays of 4×4 discrete MPPCs from Hamamatsu Photonics (S12643-050CN). They have an active chip size of 3.0×3.0 mm^2 and an inter-chip gap of 0.6 mm and are fitted with a Samtec ST4 connector. In contrast to monolithic arrays, which share a common cathode, the discrete MPPCs feature individual cathodes, thus allowing differential readout which reduces electronic cross talk as well as improves the time resolution [12]. The MPPCs used in this project exploit the through-silicon vertical-interconnect access technology, leading to less deadspace and a reduced connection length as compared to conventional wire-bonded SiPMs. They have been the result of recent developments by Hamamatsu Photonics. A mass characterisation of the MPPC arrays is currently performed in order to assure the quality of the devices as

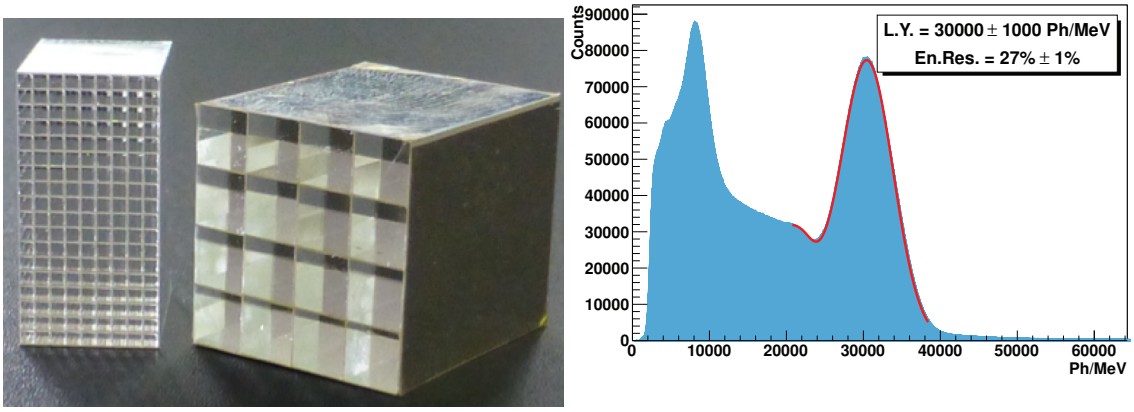

Figure 3: (*left*) Photograph of 9×18 crystal matrix for the endoscopic PET detector (the size of the single crystals is $0.71 \times 0.71 \times 15$ mm^3) and the 4×4 crystal matrix for the external detector plate. The size of the single crystals for the latter one is $3.5 \times 3.5 \times 15$ mm^3. (*right*) Energy spectrum in photons/MeV of one of the external plate crystal matrices. The fit function is a convolution of a Gaussian for the photo peak and a Fermi-Dirac function to model to Compton edge. Result obtained by one of us (M. Pizzichemi) at CERN.

well as to adjust the operation bias voltage of all individual detector channels to the same gain. A typical single photo-electron spectrum is depicted in Fig. 4 (left). It is acquired by illuminating the 16 MPPC channels with blue laser light, attenuated to low intensity to ensure single-photon detection. The MPPC is mounted on a motherboard incorporating linear amplifiers, high voltage filters and a temperature sensor. The output signal is amplified by a ten times voltage amplifier and read out by a VME-based charge-to-digital converter (QDC) with a resolution of 25 fC per QDC bin. 200k events are recorded for 20 different levels of the applied bias voltage. The signal from the MPPC is integrated in a gate with effective length of 100 ns. During the gain measurement, the gate for charge integration is synchronized with the laser pulse. In addition, for each voltage level, a measurement without light is performed in order to extract the dark count rate (DCR) and the optical cross talk. The distance between the individual peaks of the single photo-electron spectrum is defined as the gain. It is plotted as a function of the applied bias voltage in Fig. 4 (right). From a linear fit, the breakdown voltage is extrapolated as the voltage at which the gain equals to zero. The knowledge of the breakdown voltage is of importance since all channels will operate at a fixed excess bias voltage to assure a homogenous detector response to incoming photons.

3.3 Digital SiPMs

The crystal matrices of the internal probe are coupled to multi-channel digital Silicon photomultipliers (md-SiPMs) which have been custom developed within the collaboration [13, 14]. The single photon avalanche diodes (SPADs) of a md-SiPM are equipped with a one-bit counter which provides the digital count of pixels fired. In addition, they are read out column-wise with multiple time-to-digital converters (TDCs). This decreases the fill factor of the device but enables independent photon time-of-arrival measurements. The sensor is composed of 9×18 md-SiPMs or clusters, each of which contains of 16×26 SPAD pixels with a size of 30×50 μm^2. A reasonable trade-off between fill factor and number of time-over-threshold measurements leads to a number

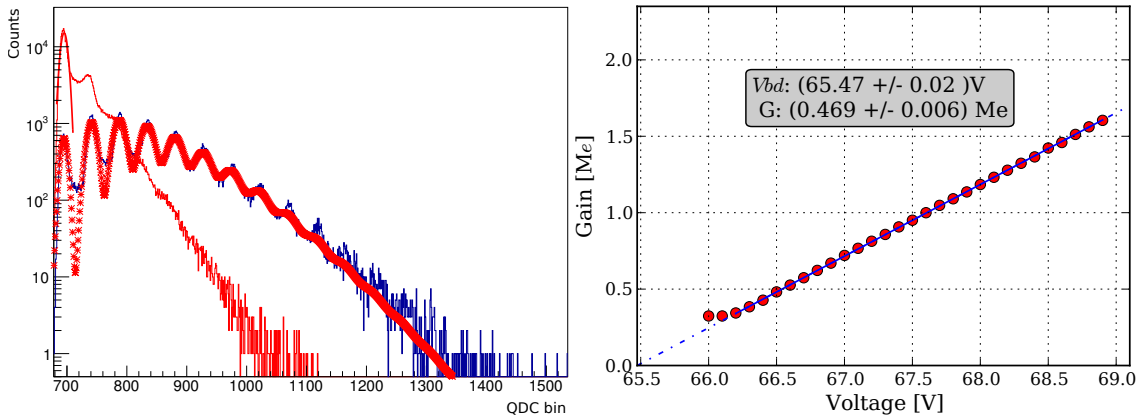

Figure 4: (*left*) Single photo-electron spectrum (blue) with a multiple Gaussian fit (red asterisks). The red histogram is a spectrum from a dark run from which DCR and cross talk can be extracted. (*right*) Gain in million electrons as a function of the applied bias voltage as extracted from the aingle photo-electron spectra. The blue line is a straight line fit on the data points whose errors are negligible on this scale. The breakdown voltage (Vbd) and gain (G) at 1 V overvoltage, obtained from the fit, are given in the inlet. Results obtained by one of us (A. Silenzi) at DESY.

of 48 TDCs per column of clusters and a fill factor of 57%. Combining the information of the different timestamps statistically ensures that the lower bound of the theoretically achievable CTR is always reached and thus improves the CTR significantly [15, 16].

The 9×18 md-SiPM chip has been fabricated and tested. It features in-situ statistical analysis of the gamma events, real-time noise rejection, a high-speed interface with the DAQ as well as multi-channel timestamping. Digital SiPMs typically suffer from high dark count rate (DCR) which, however, can be significantly reduced by cooling and by masking noisy pixels. Measurements with a test prototype suggest that the DCR at room temperature of around 40 MHz at 3 V excess bias can e.g. be reduced to 23 MHz with 10% masking. The DCR as a function of the population of active pixels is depicted in Fig. 5 (left). Such small masking levels are able to reduce the DCR significantly while having only a small impact on the photon detection efficiency (PDE), c.f. Fig. 5 (right). The time jitter for one pixel of the prototype is determined to be 104 ps FWHM. The clusters incorporate a PDE of smaller than 17% and a cross talk of smaller than 10%.

3.4 ASIC

The analog SiPMs of the external plate are read out by dedicated 64-channel ASICs. The high demands on the timing as well as the high channel density require the front-end electronics to be fast, low-noise and to cope with the expected high dark count rate of the SiPMs. Moreover, because of the high channel density of 4096 channels on 23×23 cm^2, the front-end electronics need to integrate a high number of readout channels with a limited power budget in order to minimise cooling. Since the operation voltage of the SiPMs may vary by up to 0.5 V, the ASIC needs to be able to tune the SiPM bias voltage for each individual channel by up to this amount. To fulfill these requirements, two ASIC prototypes have been developed, StiC [17] and TOFPET ASIC [18]. In both cases, the ASICs provide a fine time measurement and a time-over-threshold (ToT) measurement for each input pulse, where the latter one determines the pulse energy. The ASIC inhibits

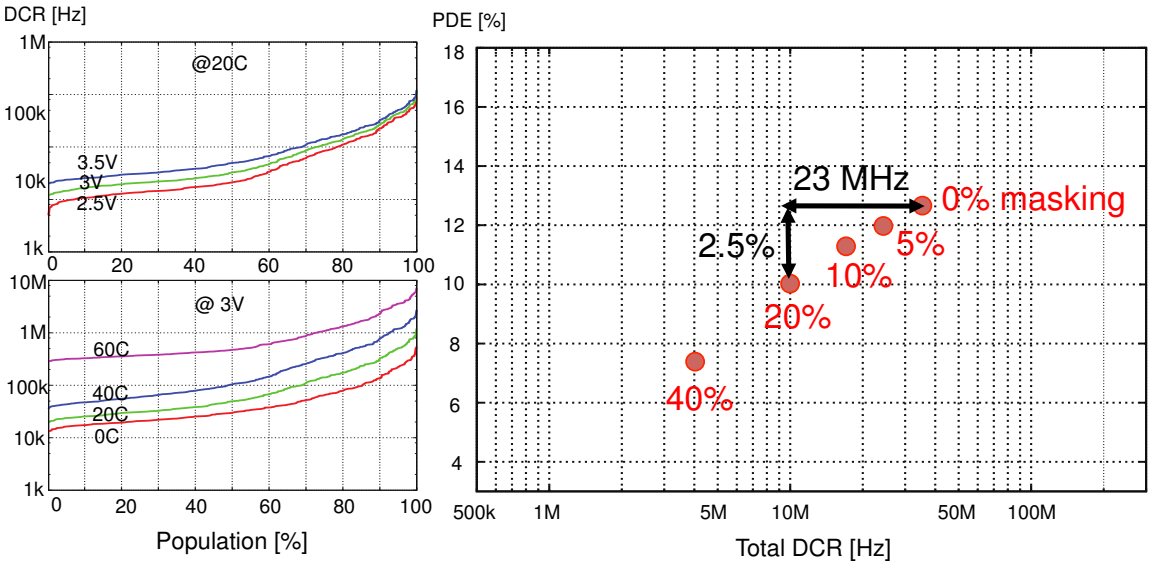

Figure 5: (*left*) Distribution of the dark count rate (DCR) of the 416 pixels for different excess bias voltages (top) and different temperatures (bottom). (*right*) The influence of different masking levels on photon detection efficiency (PDE) and integrated (total) DCR of the whole cluster [14].

a self-triggering mechanism based on a double-threshold system. For the time measurement, a low threshold is used, whereas a higher threshold accomodates for dark count rejection and ToT measurement.

The 64-channel TOFPET ASIC has been produced in 130 nm CMOS technology. The readout channel consists of an analogue front-end, combined with a mixed-signal TDC with a 50 ps resolution time stamp. Its output contains the time of the trigger as well as the time-over-threshold. The time information is extracted by applying a threshold to the leading edge of a fast signal replica. Degradation due to time-walk can be corrected offline. By applying this threshold as low as possible, down to 0.5 photoelectrons (0.5 p.e.), the scintillator-induced time jitter is overcome. A higher threshold is used to reject dark counts and provide a second time stamp for the ToT determination. The power consumption of the ASIC amounts to 7-9 mW/channel.

A 16-channel prototype of the STiC ASIC has been produced in 180 nm CMOS technology and is currently under test. The analog front-end has been tested in conjunction with a SiPM, reading out the signals from a ^{22}Na source. Both single-ended and differential readout are possible. The latter, however, seems to perform better in terms of noise rejection. The ToT output is found to depend linearly on the input charge for signals larger than 3 pC and the jitter of the trigger is less than 30 ps for signals of 3 pC. The input bias digital-to-analog converter (DAC) for the tuning of the individual SiPMs is linear within a range of 0.7 V. The TDC, with a bin size of 50 ps, is working up to specifications and is stable over a time of at least two hours. The 64-channel version of the motherboard has been taped-out and is currently under test.

4. Full System Simulation and Image Reconstruction

The EndoTOFPET-US detector system has been simulated in an environment where the emis-

sion of the photons and their passage through matter can be modelled. This includes the absorption and scattering of the photons in the body as well as in the single detector components. The simulation framework is based on the toolkit GATE v6 [19], a Geant4-based advanced open source software for simulations in nuclear medical imaging. GATE is designed for symmetrical detector systems and has been customised to accommodate for the asymmetric design of EndoTOFPET-US detector system. The simulation framework also allows for the rotation of the detectors during the data acquisition. An offline custom-made digitiser smears the exact position, time and energy information of the single events from simulation and creates physically-realistic coincidence pairs that are stored in list-mode format and can be read by the image reconstruction software.

The first figure of merit of the PET detector is its sensitivity. It is defined as the number of true coincidences divided by the number of decays. It can be seen from a full-system simulation in Fig. 6 (left) that the sensitivity increases with longer crystals. On the other hand, the coincidence time resolution (CTR) deteriorates with longer crystals (decreases by about 45 % when increasing the crystal length from 5 mm to 25 mm) [20]. As a tradeoff between optimising the sensitivity and optimising the CTR, a crystal length of 15 mm has been chosen for both the external plate as well as the probe crystals.

For the EndoTOFPET-US detector setup with the probe front face being located 12.5 mm from the source, the sensitivity amounts to about 7 cps/kBq. Due to a different solid-angle coverage, the distance between source and probe influences the sensitivity. For a very small distance between source and probe of 2.5 mm, the sensitivity can be doubled, c.f. Fig. 6 (right).

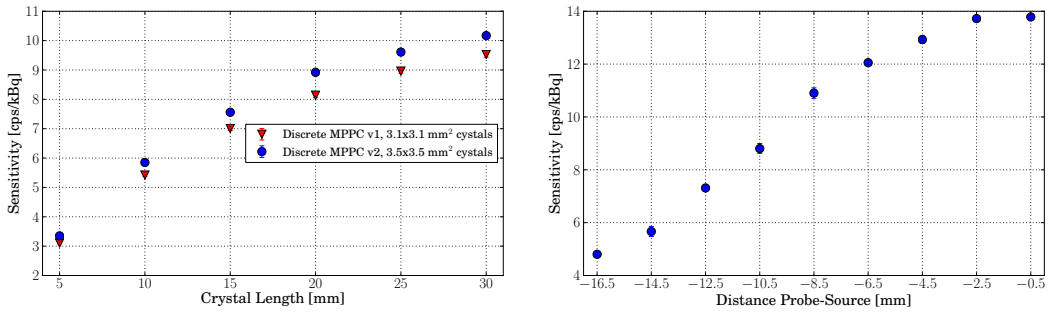

Figure 6: (*left*) Simulated full-system sensitivity as a function of the crystal length for two different SiPM models. (*right*) Simulated full-system sensitivity as a function of the distance between a point source and the probe front (for outer-plate crystals of $3.5 \times 3.5 \times 15$ mm as will be used in the final detector).

A dedicated image reconstruction software is being developed for the EndoTOFPET-US system in order to fulfil the demanding requirements. The image reconstruction is challenging due to the following reasons: First, it needs to incorporate the TOF information. Since the endoscopic detector is freehand, the volume of interest is undefined and changes continuously. PET typically suffers from low sensitivity and high noise, which is especially true for the EndoTOFPET-US system because of the limited field of view so that the reconstruction software needs to accomodate for the limited solid angle. Furthermore, the image needs to be reconstructed on-line to provide guidance for the physician, so it needs to be fast. In order to overcome these difficulties, the histogram-mode iterative maximum-likelihood expectation-maximisation (ML-EM) reconstruction method is utilised [21]. In order to solve the massively parallel problem of inverting huge matrices the com-

putation is performed on graphic processing units (GPUs). They enable a speedup by a factor of $\mathcal{O}(10)$ with respect to conventional central processing unit (CPU) computation, providing an on-line reconstructed image within the order of minutes.

The image resolution can be as low as 0.6 mm, if the size of the voxels that the region of interest is divided into is sufficiently small. Fig. 7 (centre) shows that pointsources with a radius of 1 mm can still be reconstructed with a resolution of below 1 mm if surrounded by a background activity volume with a source-to-background activity-concentration ratio of 8 : 1. The reconstructed image in Fig. 7 (right) shows the degradation of the image quality in the case of a limited rotation of only a few degrees. The resolution in y (coronal) is compatible to the full-rotation scenario while the image is blurred heavily in x.

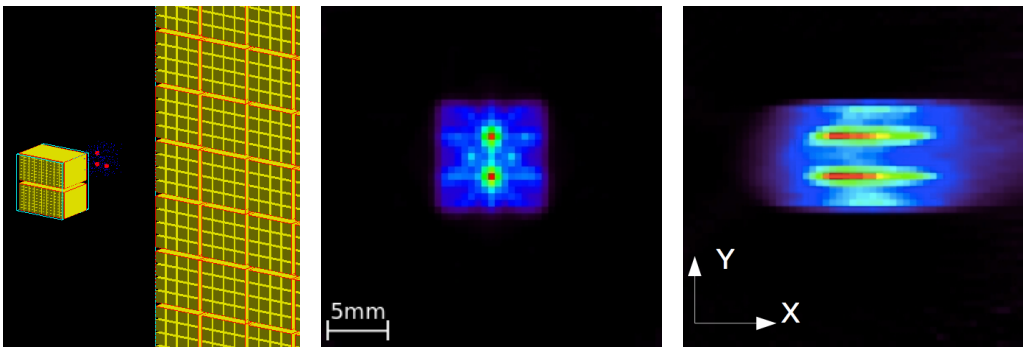

Figure 7: (*left*) GATE simulation of the detector system and a source distribution. (*center*) Reconstructed image with full rotation in 45° steps. (*right*) Reconstructed image with limited rotation.

5. Conclusion

In the scope of the EndoTOFPET-US project, a novel multimodal device for Ultrasound Endoscopy and Positron Emission Tomography is being developed. All the single components have been finalised. Comprehensive tests on the properties of the single components have been performed and confirm that the individual devices are fully functional and meet the specifications. Preliminary measurements suggest that a CTR of the order of 200 ps is within reach. Under ideal conditions, image resolutions of 0.6 mm can be achieved. The project now enters the phase of integrating the single components into a working prototype. The commissioning and the clinical tests are forseen for 2014.

Acknowledgments

The author thanks the EndoTOFPET-US collaboration for the privilege of representing it at this conference.

This research project has received funding from the European Union 7th Framework Program (FP7/ 2007-2013) under Grant Agreement No. 256984 (EndoTOFPETUS) and is supported by a Marie Curie Early Initial Training Network Program (PITN-GA-2011-289355-PicoSEC-MCNet).

References

[1] EndoTOFPET-US Proposal. Novel multimodal endoscopic probes for simultaneous PET/ultrasound imaging for image-guided interventions. *European Union 7th Framework Program (FP7/2007-2013) under Grand Agreement No. 256984, Health-2010.1.2-1*.

[2] E. Garutti. EndoTOFPET-US - A novel multimodal tool for endoscopy and Positron Emission Tomography. In *Nuclear Science Symposium and Medical Imaging Conference (NSS/MIC), 2012 IEEE*, pages 2096–2101, 2012.

[3] B. Frisch. Combining endoscopic ultrasound with Time-Of-Flight PET: The EndoTOFPET-US Project. *Nucl. Instr. Meth. A*, In press, 2013.

[4] Robert Koch-Institut (Hrsg) und die Gesellschaft der epidemiologischen Krebsregister in Deutschland e.V. (Hrsg). *Krebs in Deutschland 2007/2008, 8. Ausgabe*. Robert Koch-Institut, 2012.

[5] R. Bugalho, C. Gaston, M.D. Rolo, J.C. Silva, R. Silva, and J. Varela. EndoTOFPET-US data acquisition system. *Journal of Instrumentation*, 8(02):C02049, 2013.

[6] CAMPCom: A Lightweight and Portable Communication Framework for Multimodal Image-Guided Therapy . `http://campar.in.tum.de/Main/CAMPCom`. Accessed: 2013-08-16.

[7] A. Schoch, B. Fuerst, F. Achilles, S. Demirci, and N. Navab. A lightweight and portable communication framework for multimodal image-guided therapy. *The Sixth International Workshop on Systems and Architectures for Computer Assisted Interventions (SACAI)*, September 2013.

[8] Medical electrical equipment - part 1: General requirements for basic safety and essential performance. Norm IEC 60601-1, 2005.

[9] T. Reichl, J. Gardiazabal, and N. Navab. Electromagnetic servoing - a new tracking paradigm. *IEEE Trans. Med. Imaging*, 32(8):1526–1535, 2013.

[10] E. Auffray, F. Ben Mimoun Bel Hadj, N. Brillouet, P. Coudray, K. Doroud, G. Fornaro, B. Frisch, S. Gundacker, A. Knapitsch, P. Jarron, T. Meyer, M. Paganoni, K. Pauwels, M. Pizzichemi, M. Vangeleyn, and P. Lecoq. Design and performance of detector modules for the endoscopic PET probe for the FP7-project EndoTOFPET-US. In *Nuclear Science Symposium and Medical Imaging Conference (NSS/MIC), 2012 IEEE*, pages 3236–3240, 2012.

[11] J. Trummer, D. Aimard, E. Auffray, G. Chevenier, C. Laffay, P. Lecoq, P. Sempere-Roldan, and O. Teller. Scintillation properties of LuYAP and LYSO crystals measured with MiniACCOS, an automatic crystal quality control system. In *Nuclear Science Symposium Conference Record, 2005 IEEE*, volume 5, pages 2807–2810, 2005.

[12] K. Doroud, K. Auffray, P. Jarron, T. Meyer, and P. Lecoq. Differential readout: The technique to optimise timing in a monolithic MPPC array. *Nucl. Inst. Meth. A, 717, 5-10*, 2013.

[13] S. Mandai, V. Jain, and E. Charbon. A fully-integrated $780 \times 800 \mu m^2$ multi-digital silicon photomultiplier with column-parallel time-to-digital converter. In *Proceedings of the ESSCIRC*, pages 89–92, 2012.

[14] S. Mandai and E. Charbon. Multi-channel digital SiPMs: Concept, analysis and implementation. In *Nuclear Science Symposium and Medical Imaging Conference (NSS/MIC), 2012 IEEE*, pages 1840–1844, 2012.

[15] M. Fishburn and E. Charbon. System Tradeoffs in Gamma-Ray Detection Utilizing SPAD Arrays and Scintillators. *IEEE Trans. Nucl. Sci. Vol. 57, No. 5*, 2010.

[16] S. Seifert, H.T. van Dam, and D.R. Schaart. The lower bound on the timing resolution of scintillation detectors. *Phys Med Biol. 57 1797-1814*, 2012.

[17] W. Shen, K. Briggl, W. Chen, P. Fischer, A. Gil, T. Harion, M. Ritzert, and H.-C. Schultz-Coulon. STiC - A mixed mode chip for SiPM ToF applications. In *Nuclear Science Symposium and Medical Imaging Conference (NSS/MIC), 2012 IEEE*, pages 877–881, 2012.

[18] M.D. Rolo, R. Bugalho, F. Goncalves, G. Mazza, A. Rivetti, J.C. Silva, R. Silva, and J. Varela. TOFPET ASIC for PET applications. *Journal of Instrumentation*, 8(02):C02050, 2013.

[19] S. Jan et al. GATE: A simulation toolkit for PET and SPECT. *Phys. Med. Biol. 49 4543*, 2004.

[20] E. Garutti, K. Gadow, M. Goettlich, A. Silenzi, and Chen Xu. Single channel optimization for an endoscopic time-of-flight positron emission tomography detector. In *Nuclear Science Symposium and Medical Imaging Conference (NSS/MIC), 2011 IEEE*, pages 54–58, 2011.

[21] R.M. Lewitt and S. Matej. Overview of methods for image reconstruction from projections in emission computed tomography. *Proceedings of the IEEE*, 91(10):1588–1611, 2003.